Theoretical Study of the 1,2 Rearrangement of Housane Radical Cations: Key Role of a Transient Cyclopentane-1,3-diyl Intermediate

Lluís Blancafort,*,‡ Waldemar Adam,§ David González,‡ Massimo Olivucci,*,† Thom Vreven,‡ and Michael A. Robb*,‡

Contribution from the Department of Chemistry, King's College London, Strand, London WC2R 2LS, U.K., Institut für Organische Chemie, University of Würzburg, Am Hubland, D-97074, Würzburg, Germany, and Istituto di Chimica Organica, Università di Siena, Via Aldo Moro, 53100 Siena, Italy

Received May 3, 1999. Revised Manuscript Received September 16, 1999

Abstract: CASSCF computations suggest that the ground-state potential energy surface of housane radical cations is centered around a conical intersection (and its surrounding Jahn−Teller-type surface) at a planar, symmetric cyclopentane-1,3-diyl geometry. In our reactivity model, this region is connected to the reactants via a bridge-bending coordinate and to the products via a shift coordinate. The preference for the spin-localized planar intermediate is caused by the preferential energy stabilization along a charge localization coordinate (the derivative-coupling coordinate at the conical intersection). Mechanistically, our computations show that the reaction proceeds in two steps: the breakage of the one-electron bond of the reactants, which produces the asymmetric, quasi-planar intermediate and is the rate-determining step, and the subsequent 1,2 rearrangement, which is essentially barrierless. The reaction results in the selective 1,2 migration of the original *endo* substituent of the reactant.

Introduction

Organic radical cations are reactive intermediates which have attracted considerable attention during the past decade.[1] Their intrinsic radical character makes the study of their properties accessible through EPR spectroscopy, while their high reactivity raises the challenge of their application as efficient and selective reagents. In particular, the observed reaction selectivity and the rate of depletion suggest that radical cations often undergo fast, single-step (i.e., concerted) reactions, leading to more stable fragmented or rearranged products.

Bicyclo[2.1.0]pentane radical cations (i.e., housane radical cations) are highly reactive intermediates and undergo a sigmatropic-like hydrogen or alkyl 1,2 shift with great selectivity to produce more stable olefinic radical cations.[2] As shown in Scheme 1, the housane radical cations are usually produced by γ radiolysis and chemical or photochemical electron-transfer reactions of bicyclo[2.1.0]pentanes and 2,3-diazabicyclo[2.2.1]-heptanes. After rearrangement and back electron transfer, these yield the corresponding olefins, a transformation that has proved to be useful for the synthesis of diquinanes and other polycyclic hydrocarbons.[2d] The mechanism of the sigmatropic-like hydrogen or alkyl shift in these radical cations raises some interesting questions: Is this pericyclic-like reaction concerted, or is it stepwise? How does the distinctive reaction coordinate of a radical cation sigmatropic shift differ from that of a neutral species? Are the transition-state structures and minima which control the reactivity and selectivity of the reaction asymmetric, and can this fact be related to a crossing of states (conical intersection), as shown by Bally and Cársky for the potential energy surface of cyclobutene and bicyclobutane radical cations ($C_4H_6^{\bullet+}$)?[3]

Scheme 1

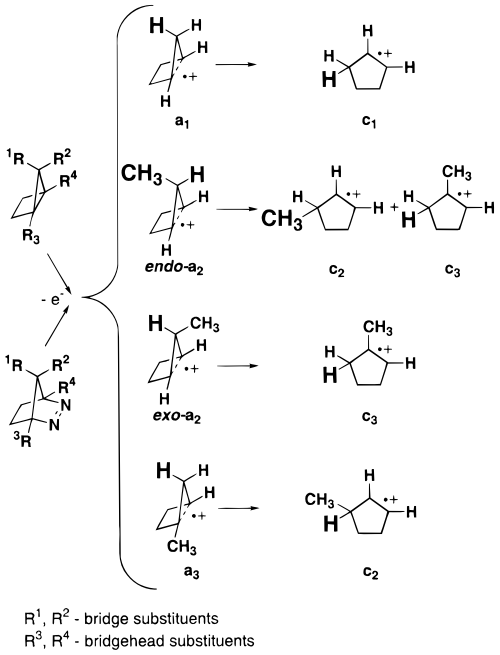

The main experimental features of housane radical cations can be reviewed with the help of Schemes 1 and 2. Experimental

‡ King's College London.
§ University of Würzburg.
† Università di Siena.

(1) For a recent review, cf.: Schmittel, M.; Burghart, A. *Angew. Chem., Int. Ed. Engl.* **1997**, *36*, 2551−2589.

(2) (a) Williams, F.; Guo, Q.-X.; Kolb, T. M.; Nelsen, S. F. *J. Chem. Soc., Chem. Commun.* **1989**, 1835−1837. (b) Adam, W.; Walter, H.; Chen, G.-F.; Williams, F. *J. Am. Chem. Soc.* **1992**, *114*, 3007−3014. (c) Adam, W.; Sahin, C.; Sendelbach, J.; Walter, H.; Chen, G.-F.; Williams, F. *J. Am. Chem. Soc.* **1994**, *116*, 2576−2584. (d) Adam, W.; Heidenfelder, T.; Sahin, C. *Synthesis* **1995**, 1163−1170. (e) Adam, W.; Corma, A.; Miranda, M. A.; Sabater-Picot, M. J.; Sahin, C. *J. Am. Chem. Soc.* **1996**, *118*, 2380−2386. (f) Adam, W.; Handmann, V.-I.; Kita, F.; Heidenfelder, T. *J. Am. Chem. Soc.* **1998**, *120*, 831−832. (g) Adam, W.; Heidenfelder, T. *J. Am. Chem. Soc.* **1998**, *120*, 11858−11863.

10.1021/ja991441p CCC: $18.00
Published on Web 11/03/1999

Scheme 2

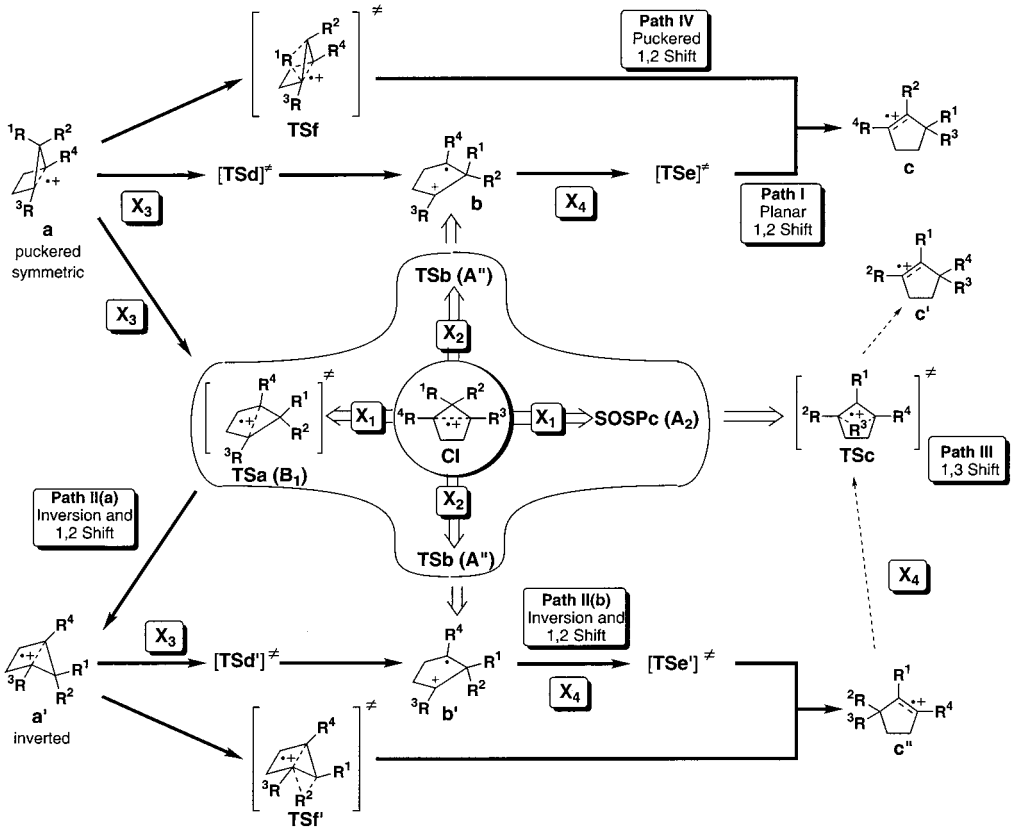

results are available for the parent molecule $\mathbf{a_1}$ (notation given in Scheme 1, where the subscripts refer to the substitution pattern) and its methyl-substituted derivatives ***endo*-$\mathbf{a_2}$** (*endo* methyl substituent at the bridge), ***exo*-$\mathbf{a_2}$** (*exo* methyl substituent at the bridge), and $\mathbf{a_3}$ (methyl substituent at the bridgehead).[2a−c] Although the 1,3 radical cations are highly reactive, EPR spectra of the 1,3 species could be recorded in a matrix (77 K) for the unsubstituted reactant $\mathbf{a_1}$ and the bridge-substituted ***endo*-$\mathbf{a_2}$** and ***exo*-$\mathbf{a_2}$**, but not for the bridgehead methyl-substituted $\mathbf{a_3}$. These results imply that the barriers associated with the 1,2 migration (path I, Scheme 2) must be higher for molecules $\mathbf{a_1}$ and $\mathbf{a_2}$ than for $\mathbf{a_3}$, and the results of our computations will elucidate the origin of this behavior.

The selectivity of the 1,2 rearrangement is the crucial characteristic of the reactivity, since it renders the reaction synthetically useful. It has been experimentally established that it is the *endo* substituent (R^1) which migrates stereoselectively. Thus, hydrogen migration was observed for substrates $\mathbf{a_1}$, ***exo*-$\mathbf{a_2}$**, and $\mathbf{a_3}$, while methyl migration was the main product for the rearrangement of ***endo*-$\mathbf{a_2}$** at low temperatures (cf. Scheme 1). Moreover, extensive experimental studies[2] have proven that the regioselectivity of the migration is dictated by the stabilization of the positive charge and the spin density at the bridgehead positions by the substituents R^3 and R^4. The experimental evidence establishes that the migration occurs to the bridgehead atom with the highest positive charge, regardless of thermodynamic factors. This feature is exemplified by our asymmetric substrate $\mathbf{a_3}$, for which experimentally only regioisomer $\mathbf{c_2}$ (formed after migration to the methyl-substituted carbon) and not the thermodynamically favored $\mathbf{c_3}$ was obtained (cf. Scheme 1).

In this paper, we have documented computationally (i) a concerted and stepwise sigmatropic-like 1,2 shift, (ii) a concerted sigmatropic-like 1,3 shift, and (iii) the bicyclo[2.1.0]pentane ring-inversion path. Our results suggest that the housane radical cations undergo a peculiar conformational change which results in the production of a short-lived cyclopentane-1,3-diyl *planar intermediate* (see structure **b** in Scheme 2), which subsequently evolves, via a hydrogen or alkyl 1,2 shift, toward an olefinic product (see structure **c** in Scheme 2). Therefore, our results indicate that the sigmatropic shift reactions in bicyclo[2.1.0]-pentane radical cations are either two-step or highly asynchronous one-step processes (see path I in Scheme 2), depending on the substituents. The concerted process (see path IV in Scheme 2), as well as the other potentially competitive processes (see paths II and III in Scheme 2), are not active due to the larger reaction energy barriers. The magnitudes of the computed energy barriers along path I indicate that formation of the planar cyclopentane-1,3-diyl intermediate **b** is the *rate-determining* step of the sigmatropic-like reaction and thus provides the essential potential energy surface feature for the rationalization and control of the reactivity of housane radical cations.

Our computations also provide a fully documented example of an organic molecule whose ground-state potential energy surface topology is centered around a conical intersection (**CI** in Scheme 2) and its surrounding Jahn−Teller-type surface (see the framed region in Scheme 2). Similar situations have been described by Davidson et al. for the structure of 1,3 dimethylene-cyclobutadiene,[4a] methane radical cation,[4b] and the reactivity of formyloxyl radical[4c] and more recently by Bally, Càrsky, et al.[3] for the potential energy surface of $C_4H_6^{\bullet+}$. In what follows,

(3) Sastry, G. N.; Bally, T.; Hrouda, V.; Cársky, P. *J. Am. Chem. Soc.* **1998**, *120*, 9323−9334.

(4) (a) Davidson, E. R.; Borden, W. T.; Smith, J. *J. Am. Chem. Soc.* **1978**, *100*, 3299−3303. (b) Katriel, J.; Davidson, E. R. *Chem. Phys. Lett.* **1980**, *76*, 259−262. (c) Feller, D.; Huyser, E. S.; Borden, W. T.; Davidson, E. R. *J. Am. Chem. Soc.* **1983**, *105*, 1459−1466.

we will provide evidence that the key mechanistic role of the planar cyclopentane-1,3-diyl intermediate is intimately related to the "global structure" of the potential energy surface, i.e., to the planar Jahn−Teller-like region and its connection to the regions of reactant and product.

As illustrated in Scheme 2, the Jahn−Teller-like region is defined by two different geometrical coordinates, indicated as $\mathbf{X_1}$ and $\mathbf{X_2}$ (the gradient difference and derivative coupling coordinates, whose definition is given in the following subsection).[5,6] Now, the main reaction path I begins with the breaking of the one-electron σ bond in the puckered housane radical cation reactant (**a** in Scheme 2), followed by the planarization of the ring, leading to the Jahn−Teller-like region. From the planar region, the 1,2-hydrogen or -alkyl shift to the product is computed to be essentially barrierless. Thus, the reaction mechanism can be rationalized in terms of the four coordinates shown in Scheme 2: the two directions $\mathbf{X_1}$ and $\mathbf{X_2}$ that define the space of the "moat" associated with the conical intersection; $\mathbf{X_3}$, the ring-puckering coordinate that connects the housane radical cation with the Jahn−Teller-like region of Scheme 2; and $\mathbf{X_4}$, the hydrogen or alkyl shift coordinate that connects the Jahn−Teller-like region to the reaction product.

Theoretical Considerations

There is an important relationship between the electronic and molecular structure of the planar cyclopentane-1,3-diyl transient species (which is an energy minimum on the potential energy surface) and the structure corresponding to a conical intersection of C_{2v} symmetry, where the bonding ground state ($^2B_1$) and the antibonding excited state ($^2A_2$) of the system are degenerate (a "cusp" on the ground-state potential energy surface).[7] The state crossing results from a change from the dominant through-space interaction between C_1 and C_3 at puckered geometries, which favors the bonding $^2B_1$ state, to a dominant through-bond interaction at planar geometries, which favors the antibonding $^2A_2$ state. The computations show that the cyclopentane-1,3-diyl structure (structure **b** in Scheme 2) is "generated" by distorting the conical intersection structure along a symmetry-breaking coordinate, dominated by an asymmetric ring-stretching mode. As we shall presently discuss, one rigorous way of understanding this feature is that the transient intermediate is located near the classic "moat" (indicated as the framed region in Scheme 2) of a two-dimensional "Mexican hat" or Jahn−Teller-like energy surface structure encountered for degenerate states in tri- or tetra-atomic systems.[8]

The basic qualitative features of the topology of the Jahn−Teller-like surface, which surrounds the conical intersection (**CI**) as presented in Scheme 2, can be predicted a priori from simple group-theoretical arguments. As Davidson showed for polyatomic potential surfaces,[5] there are two directions, $\mathbf{X_1}$ and $\mathbf{X_2}$, which lift the degeneracy as one distorts the geometry from the apex of the cone **CI** in Scheme 2. These are the gradient difference vector (eq 1),

$$\mathbf{X_1} = \frac{\partial(E_1 - E_2)}{\partial \mathbf{Q}} \tag{1}$$

where E_1 and E_2 are the energies of the degenerate states, and the gradient of the interstate coupling vector (eq 2),

$$\mathbf{X_2} = \left\langle \Psi_1 \left| \frac{\partial H}{\partial \mathbf{Q}} \right| \Psi_2 \right\rangle \tag{2}$$

where Ψ_1 and Ψ_2 are the wave functions of the states. In eqs 1 and 2, H is the Hamiltonian, and $\mathbf{Q}$ represents the nuclear configuration vector of the system. It follows from group-theoretical arguments that, if Ψ_1 and Ψ_2 have different symmetry ($^2B_1/^2A_2$), then $\mathbf{X_1}$ must be totally symmetric (a_1) and $\mathbf{X_2}$ must be nontotally symmetric (b_2). In the space of planar geometries, the totally symmetric (a_1) coordinate $\mathbf{X_1}$ must be dominated by the 1,3 carbon−carbon bond stretch (or, equivalently, the symmetric $C_1 \leftarrow C_2 \rightarrow C_3$ stretch, cf. Figure 1a). Similarly, the non-totally symmetric $\mathbf{X_2}$ coordinate (which must have symmetry b_2) corresponds to the asymmetric $C_1 \rightarrow C_2 \rightarrow C_3$ stretch (cf. Figure 2a). As illustrated in Scheme 2, one must be able to find symmetry-constrained minima in the space of displacements along $\mathbf{X_1}$ and $\mathbf{X_2}$. These minima will have one or more directions of negative curvature (i.e., imaginary frequencies) in coordinates orthogonal to $\mathbf{X_1}$ and $\mathbf{X_2}$. Therefore, along the totally symmetric (a_1) $\mathbf{X_1}$ coordinate, one should find a symmetry-constrained minimum on the $^2B_1$ bonding branch of the Jahn−Teller surface with a short C_1-C_3 bond distance and a minimum on the antibonding $^2A_2$ branch with a long C_1-C_3 bond distance (cf. Figure 1b). It can also be expected that the unpaired electron will localize as one distorts along the $C_1 \rightarrow C_2 \rightarrow C_3$ b_2 stretch coordinate $\mathbf{X_2}$ (cf. Figure 2b). Now we must have two equivalent $^2A''$ stationary points with localized electrons on the carbon centers 1 or 3. The chemical role of the symmetry-constrained minima can be determined only by the actual computations, which we shall discuss in detail subsequently. However, this type of surface topology must[9] exist a priori, and only actual computation can determine the "depth" of the moat and establish the possible role of nonadiabatic effects.

The surface topology of the moat can explain possible theoretical problems in previous computations of radical cations. Inadequate theoretical methods, when used in the vicinity of a near degeneracy, have caused some difficulties in previous theoretical treatments of related problems. Ab initio studies on the related cyclopropane[10] and bicyclobutane[3,11] radical cations were plagued by the problems of spin contamination and spurious symmetry breaking and were very sensitive to the basis set and the level of theory. In the case of the planar cyclopropane radical cation (the trimethylene radical cation), although detailed MP2/6-31G* investigations have established that it is not a stable intermediate in the 1,2 H shift of cyclopropyl radical cations,[10b] its chemical role has not been satisfactorily clarified. For the

(5) Davidson, E. R. *J. Am. Chem. Soc.* **1977**, *99*, 397−402.

(6) For recent reviews, cf.: (a) Klessinger, M.; Michl, J. *Excited States and Photochemistry of Organic Molecules*; VCH: New York, 1995; pp 183−184. (b) Bernardi, F.; Olivucci, M.; Robb, M. A. *Chem. Soc. Rev.* **1996**, *25*, 321−328.

(7) We refer here to the $^2B_1$ state as bonding and the $^2A_2$ state as antibonding because they correlate with the $^2A'$ (bonding) and $^2A''$ (antibonding) states of the puckered reactant $\mathbf{a_1}$, respectively. Since the $^2A'$ and $^2A''$ states are the ground and excited states of $\mathbf{a_1}$, we also refer to $^2B_1$ and $^2A_2$ as the ground and excited states.

(8) Herzberg, G. *Electronic Spectra of Polyatomic Molecules*; Van Nostrand: New York, 1966; pp 48 and 449.

(9) (a) Teller, E. *J. Phys. Chem.* **1937**, *41*, 109. (b) Herzberg, G.; Longuet-Higgins, H. C. *Discuss. Faraday Soc.* **1963**, *35*, 77.

(10) (a) Wayner, D. D. M.; Boyd, R. J.; Arnold, D. R. *Can. J. Chem.* **1985**, *63*, 3283−3289. (b) Du, P.; Hrovat, D. A.; Borden, W. T. *J. Am. Chem. Soc.* **1988**, *110*, 3405−3412. (c) Krogh-Jespersen, K.; Roth, H. D. *J. Am. Chem. Soc.* **1992**, *114*, 8388−8394. (d) Hudson, C. E.; Giam, C. S.; McAdoo, D. J. *J. Org. Chem.* **1993**, *58*, 2017−2019. (e) Skancke, A. *J. Phys. Chem.* **1995**, *99*, 13886−13889. (f) Dinnocenzo, J. P.; Zuilhof, H.; Liebermann, D. R.; Simpson, T. R.; McKechney, M. W. *J. Am. Chem. Soc.* **1997**, *119*, 994−1004.

(11) (a) Hoz, S.; Basch, H.; Cohen, D. *J. Am. Chem. Soc.* **1987**, *109*, 6891−6892. (b) Gerson, F.; Qin, X.-Z.; Ess, C.; Kloster-Jensen, E. *J. Am. Chem. Soc.* **1989**, *111*, 6456−6457. (c) Bally, T. *Theochem* **1991**, *227*, 249−264.

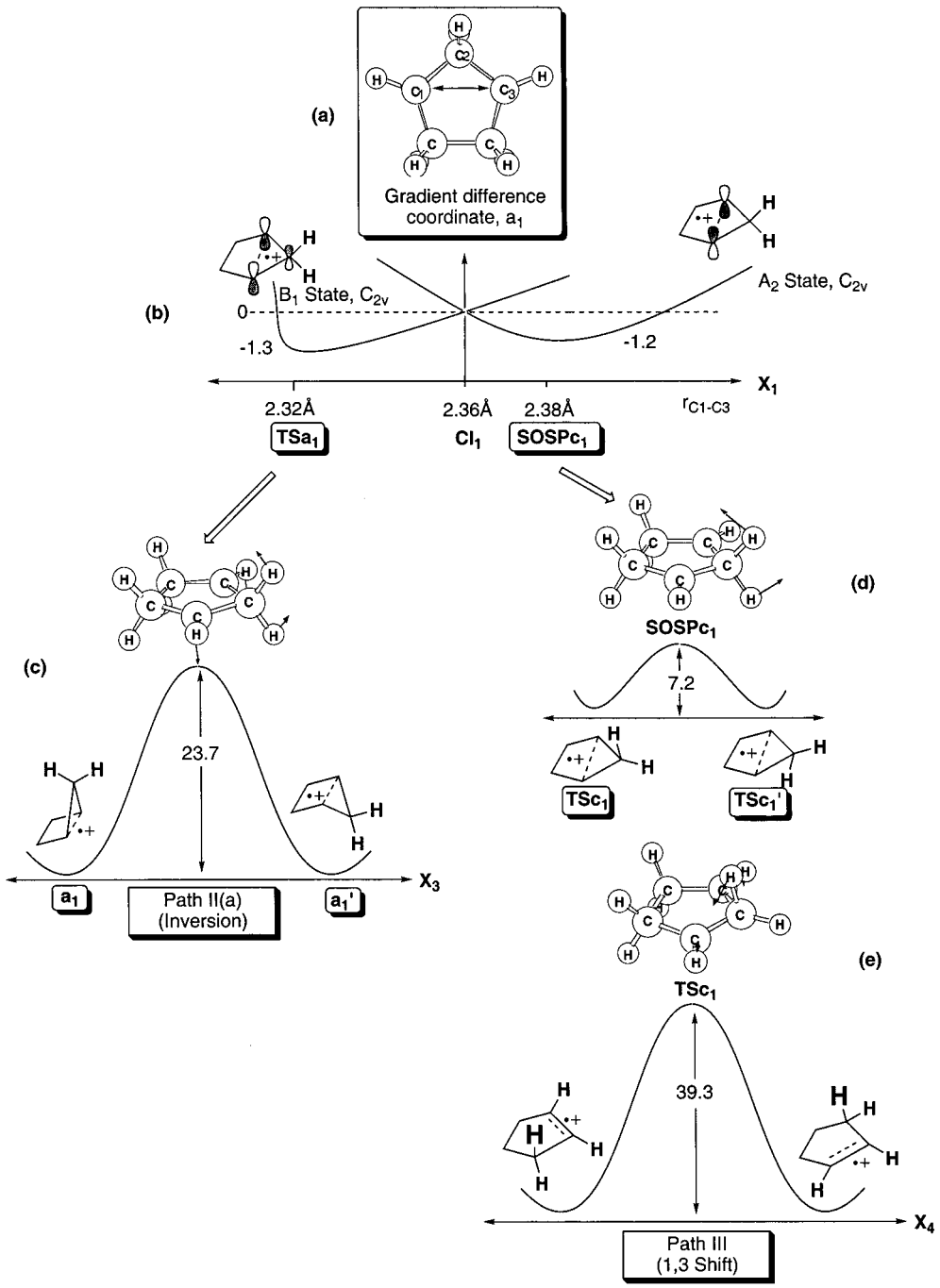

Figure 1. Branching of the Jahn−Teller-type potential energy surface along the gradient difference coordinate $\mathbf{X_1}$ for the unsubstituted cyclopentane-1,3-diyl radical cation (CASSCF(5,6)/6-31G* energies in kcal mol^{-1}).

bicyclobutyl radical cation, the planar conformer was predicted to be the transition structure for the inversion reaction, but the corresponding structure could not be obtained at the MP2 level of theory.[11c] While distorted structures were predicted by invoking the second-order Jahn−Teller effect,[10b,11c] which applies in molecules with low-lying excited diabatic states,[12] only symmetric structures were found at the MP2/6-31G* level. The origin of the computational difficulties clearly lies in the near degeneracy of the bonding (π) $^2B_1$ state and the antibonding (π^*) $^2A_2$ states.

It is clear that the region of near degeneracy near the apex of the cone can be studied only with a method (such as CASSCF) that is capable of yielding a balanced representation of the $^2B_1$/$^2A_2$ states. Further, state-averaged orbitals are essential to enforce orbital orthogonality and thus avoid spontaneous (and spurious) localization of the orbitals. As one moves away from the apex of the cone, provided one uses symmetry-adapted orbitals, then convergence to the $^2B_1$ or $^2A_2$ states can be obtained using single-reference methods. In this case, the wave functions (i.e., the inactive core orbitals) for the $^2B_1$ and $^2A_2$ states are nonorthogonal. This is of no consequence if one is interested only in the ground state. However, to maintain a balanced description of both states in the "moat" region, state-averaged CASSCF is still required. Thus, to document the surface topology in the region of near degeneracy for both ground and excited states, state-averaged CASSCF has been used in this study. For the ground-state surface as a whole, then, single-reference correlated methods are adequate and have been used in the remainder of this work.

(12) Pearson, R. G. *J. Am. Chem. Soc.* **1969**, *91*, 4947−4955.

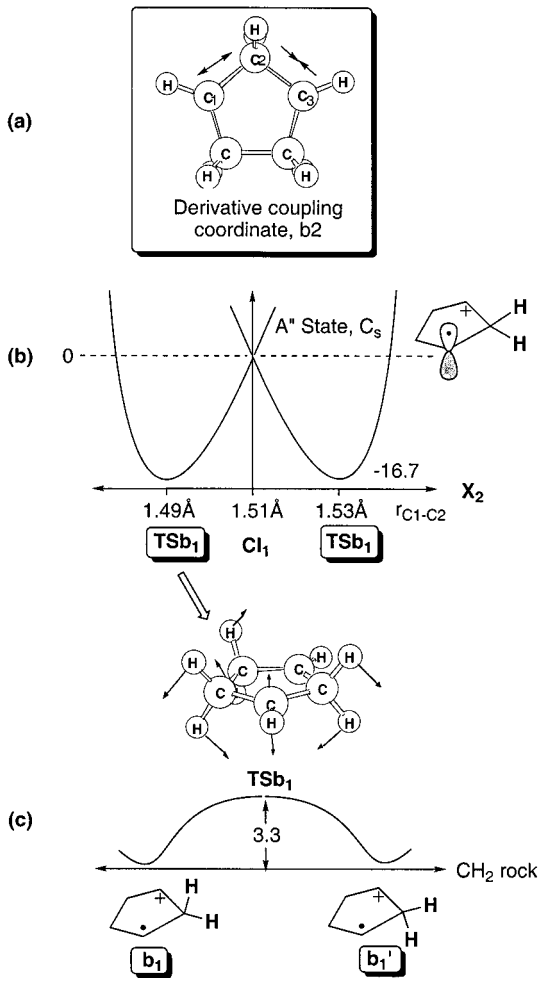

Figure 2. Branching of the Jahn−Teller-type potential energy surface along the derivative coupling coordinate $\mathbf{X_2}$ for the unsubstituted cyclopentane-1,3-diyl radical cation (CASSCF(5,6)/6-31G* energies in kcal mol^{-1}).

Results and Discussion

Our computational strategy has two objectives: (1) characterization of the topology of the moat for the Jahn−Teller-type surface that surrounds the conical intersection (the framed region of Scheme 2) and (2) a quantitative description of the reaction paths I and IV (Scheme 2). For the first objective, CASSCF-(5,6)/6-31G* optimizations were used, and all critical points have been characterized. For the second objective, the planar intermediates have been reoptimized at the UMP2/6-31G* level and connected with the reactants **a** and the products **c** by optimizing the corresponding transition structures. Careful attention has been paid to possible spin contamination, which can lead to artifacts.[13] The computed MP2 values of $\langle S^2 \rangle$ did not exceed 0.784 (cf. Tables 3 and 4, Supporting Information), which indicates that the MP2 wave functions are not significantly affected by spin contamination (expected $\langle S^2 \rangle$ value of 0.75 for radicals). Further, the energetics have been recomputed with QCISD/6-31G* single-point calculations (paths I and IV), which are referred to as MP2//QCISD throughout the text. We begin the analysis with the moat of the conical intersection.

1. CASSCF Characterization of the Moat for the Conical Intersection (CI). In this section, we describe our study of the Jahn−Teller-like topology for the parent substrate $\mathbf{a_1}$ using the CASSCF(5,6)/6-31G* level of theory (cf. Table 2, Supporting Information, for a documentation of the CASSCF active spaces used). Figures 1 and 2 show the topology of each of the critical points of the moat in the coordinates $\mathbf{X_3}$ (bridge bending) and $\mathbf{X_4}$ (hydrogen or alkyl shift) (Figure 1) and the CH_2 rock coordinate (Figure 2). (The energies of the structures are collected in Table 2, Supporting Information, together with the Cartesian coordinates. The labels refer to the structures shown in Scheme 2. For a detailed description of the Jahn−Teller-like region for the methyl-substituted derivative $\mathbf{a_2}$, the reader is referred to the Supporting Information.)

The hub of the Jahn−Teller-like topology is the optimized conical intersection of C_{2v} symmetry, $\mathbf{CI_1}$, where the bonding ($^2B_1$) and antibonding ($^2A_2$) states are degenerate. Structure $\mathbf{CI_1}$ is located 25.0 kcal/mol above the puckered minimum $\mathbf{a_1}$ (cf. Table 2, entry 3, Supporting Information). The totally symmetric coordinate $\mathbf{X_1}$ (Figure 1a) is a stretching of the C_1-C_3 bond that leads to the C_{2v}-constrained minima $\mathbf{TSa_1}$ and $\mathbf{SOSPc_1}$ (Figure 1b), which in turn have been characterized by analytical frequency calculations. $\mathbf{TSa_1}$ is the C_{2v}-constrained minimum in the "moat" for the bonding ($^2B_1$) state, where the C_1-C_3 bond is shortened from 2.36 Å in the conical-intersection structure to 2.32 Å (cf. Figure 1b). $\mathbf{TSa_1}$ has one imaginary frequency (−290 cm^{-1}), the bending of the methylene bridge (cf. Figure 1c), and acts as the transition structure for the conformational inversion of the puckered structure $\mathbf{a_1}$ along the coordinate $\mathbf{X_3}$ (cf. Figure 1c and Scheme 2). The CASSCF activation energy for the conformational inversion is 23.7 kcal/mol (cf. Table 2, entry 4, Supporting Information).

In the opposite direction, along the gradient difference coordinate $\mathbf{X_1}$, a C_{2v}-constrained minimum for the antibonding ($^2A_2$) state was found in which the C_1-C_3 distance had increased to 2.38 Å (Figure 1b). The stationary point has two imaginary frequencies (cf. Figure 1d,e), and we refer to it loosely as a second-order saddle point, denoted as $\mathbf{SOSPc_1}$. The first imaginary frequency (−360 cm^{-1}) involves the rocking of the methylene bridge and leads to two equivalent transition structures of C_s symmetry, denoted by $\mathbf{TSc_1}$ and $\mathbf{TSc_1'}$ (Figure 1d), which belong to the antibonding A″ electronic state. One of the bridge hydrogens of $\mathbf{TSc_1}$ is equatorial to the ring, while the other hydrogen is axial. The imaginary frequency of $\mathbf{TSc_1}$ (−3460 cm^{-1}) corresponds to a shift of the axial bridge hydrogen between the radical cation carbon atoms along the coordinate $\mathbf{X_4}$ (cf. Figure 1e). This frequency is also the second imaginary frequency of $\mathbf{SOSPc_1}$. Therefore, $\mathbf{TSc_1}$ is the transition structure for a degenerate isomerization of the olefinic radical cation $\mathbf{c_1}$ in the form of a suprafacial 1,3 H shift (cf. Scheme 2). The CASSCF activation energy of 39.3 kcal/mol (cf. Table 2, entry 7, Supporting Information) agrees qualitatively with the computed MP2/6-31G* barrier for the analogous reaction in propene radical cation (29.6 kcal/mol),[14] although our value is higher. The height of the activation barrier confirms that no thermal 1,3 shift of the 1,2 radical cations is likely to occur at room temperature.

Now let us consider the critical points that lie along the derivative coupling coordinate $\mathbf{X_2}$, of b_2 symmetry (Figure 2a). Motion along the coordinate $\mathbf{X_2}$ induces an asymmetric distortion of the C−C bond lengths and the localization of the spin density on one of the carbons (cf. Figure 2b). This distortion leads to two equivalent stationary points, $\mathbf{TSb_1}$, of C_s symmetry. The bond between C_2 and C_1, the spin-bearing carbon atom, is elongated from 1.51 (at $\mathbf{CI_1}$) to 1.53 Å. In contrast, the bond between C_2 and C_3, the carbon atom which bears the positive charge, is shortened to 1.49 Å. A frequency calculation on $\mathbf{TSb_1}$

(13) Bally, T.; Borden, W. T. *Rev. Comput. Chem.* **1998**, *13*, 1−97.

(14) Clark, T. *J. Am. Chem. Soc.* **1987**, *109*, 6838−6840.

shows one imaginary frequency (-171 cm^{-1}) corresponding to a rocking of the methylene hydrogen atoms (Figure 2c). This vibration leads to two equivalent, quasi-planar minima, $\mathbf{b_1}$ and $\mathbf{b_1}'$ (cf. Figure 2c), and causes the pyramidalization of the spin-bearing carbon. However, the atom which bears the positive charge remains planar, and so $\mathbf{b_1}$ has a twisted conformation in which one of the bridge substituents is axial and the other is equatorial to the ring. The CASSCF energy barrier for the

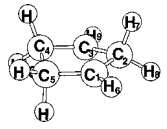

Structure $\mathbf{b_1}$

inversion of $\mathbf{b_1}$ is 3.3 kcal/mol (cf. Figure 2c and Table 2, entry 6, Supporting Information). The preference for an asymmetric structure at planar geometries is now clear. Displacement from the conical intersection along the derivative coupling coordinate $\mathbf{X_2}$ distorts the geometry, which lowers the symmetry and allows the mixing of the degenerate states with a concomitant localization of the charge.

2. 1,2 Rearrangement of the 1,3 Radical Cations $\mathbf{a_1}-\mathbf{a_3}$. 2.1. Mechanistic Rationalization of the Selectivity of the Rearrangement (Path I). In this section, we shall present the quantitatively accurate energies for the two transition structures **TSd** and **TSe** that interconnect the reactants **a** and the products **c** through the intermediates **b**, giving a complete description of the energetics of the 1,2-rearrangement path I of Scheme 2 (cf. Table 2, Supporting Information, for the corresponding CASSCF-optimized structures). Additionally, we will document the energies for the alternative, puckered rearrangement **TSf** (path IV), which confirm that the low-energy 1,2 shift for the planar structure (path I) is the preferred rearrangement process.

The puckered $\mathbf{a_1}-\mathbf{a_3}$ and quasi-planar twisted minima $\mathbf{b_1}$ and $\mathbf{b_3}$ were reoptimized at the MP2/6-31G* level of theory. The puckered conformers $\mathbf{a_1}$ and ***endo***-,***exo***-$\mathbf{a_2}$ have C_s symmetry (cf. Scheme 1) and a symmetric (or, in the case of the methyl-substituted $\mathbf{a_3}$, almost symmetric) spin density and charge distribution (cf. Table 3, entries 1, 4, and 5, Supporting Information). In all four puckered structures, the unpaired electron forms a σ one-electron bond between the 1,3 radical cationic centers, as expressed by the distances of 1.82−1.85 Å and the spin density distributions. This partial bond has been well established in ethane, cyclopropane, and bicyclobutane radical cations, for which the MP2/6-31G*-optimized C−C distances are 1.92,[15] 1.83,[10c] and 1.67 Å.[11c] The MP2-optimized geometries of the localized, quasi-planar twisted intermediates $\mathbf{b_1}$ and $\mathbf{b_3}$ were similar to the CASSCF optimized ones, and the spin density was localized on the pyramidalized carbon atom.

To complete the planar 1,2 shift (reaction path I), the two transition structures **TSd** and **TSe** were optimized with the CASSCF and MP2 methods, and the energies were recomputed with CAS-MP2 and QCISD single-point calculations, respectively (cf. Tables 1 and 4, Supporting Information). The reaction profile for the unsubstituted derivative $\mathbf{a_1}$ is summarized in Figure 3. $\mathbf{TSd_1}-\mathbf{TSd_3}$ are the transition structures for the opening of the puckered minima **a**. This process corresponds to breakage of the σ one-electron bond coupled with the localization of charge. For the parent molecule $\mathbf{a_1}$, the computed activation barriers are 13.0 and 11.9 kcal mol^{-1} at the MP2 and CAS-MP2 levels (cf. Table 1, entry 2). However, the

(15) Ioffe, A.; Shaik, S. *J. Chem. Soc., Perkin Trans. 2* **1993**, 1461−1473.

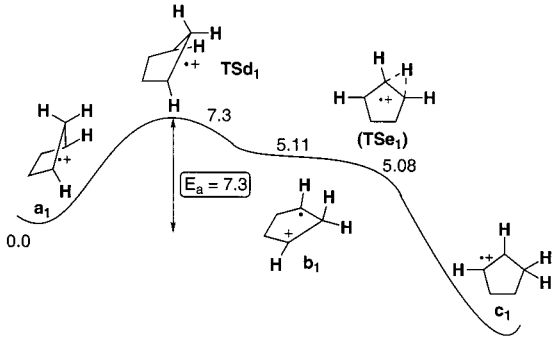

Figure 3. QCISD//MP2/6-31G* reaction coordinate for the hydrogen shift of the parent radical cation $\mathbf{a_1}$ (relative energies in kcal mol^{-1}).

Table 1. Relative Energies of the Reaction Paths I and IV for the Parent System $\mathbf{a_1}$

entry	radical cation	E_{rel} (kcal mol^{-1}) CASSCF[a]	CAS-MP2[b]	MP2[a]	QCISD//MP2[b]
1	$\mathbf{b_1}$[c]	+5.0	+5.627	+7.5	+5.1
2	$\mathbf{TSd_1}$[c]	+10.7	+11.9	+13.0	+7.3
3	$\mathbf{TSe_1}$[d]	−0.9	+0.007	+0.08	−0.03
4	***endo*-$\mathbf{TSf_1}$**[c]	+48.0	+47.1	+41.7	+44.8
5	***exo*-$\mathbf{TSf_1}$**[c]	+54.7		+47.8	

[a] Optimized geometries. [b] QCISD single-point calculations on the MP2-optimized structures. [c] Relative to the puckered conformer $\mathbf{a_1}$. [d] Relative to the twisted conformer $\mathbf{b_1}$; cf. text for the negative energies.

single-point QCISD//MP2 computations improve this value to 7.3 kcal mol^{-1}, which reproduces the experimental estimation of approximately 7 kcal mol^{-1}.[2b] This suggests that the QCISD//MP2 methodology is adequate for our studies along this reaction path, and these values are the ones we will refer to during our subsequent discussion.

For substrate $\mathbf{a_1}$, the breakage of the one-electron bond is the rate-determining step in path I. From the quasi-planar minimum $\mathbf{b_1}$, the 1,2 migration is an essentially barrierless process, and the MP2 and CAS-MP2 barriers for the migration $\mathbf{TSe_1}$ are only 0.08 and 0.01 kcal/mol (cf. Table 1, entry 3). However, the single-point QCISD//MP2 calculation gave an energy for $\mathbf{TSe_1}$ which was 0.03 kcal lower than that for the planar minimum $\mathbf{b_1}$ (note the negative value for entry 3 in Table 1); this is an artifact of the low barrier of the reaction and indicates that the structures need to be reoptimized at the QCISD level of theory (cf. Figure 3). For the bridge-substituted methyl derivatives ***endo***- and ***exo***-$\mathbf{a_2}$, no planar minima of the $\mathbf{b_2}$ type could be optimized at the MP2 level. Instead, ***endo***- and ***exo***-$\mathbf{TSd_2}$ led directly to the olefinic radical cations $\mathbf{c_2}$ and $\mathbf{c_3}$, as shown by an IRC calculation for ***exo***-$\mathbf{TSd_2}$ (cf. Figure 4).

The low 1,2 shift activation barriers for the planar conformers are caused by the twisted conformation and the localization of the C_1-C_3 orbitals as p-type on each of the carbon centers (cf. Figure 5), as indicated by the spin densities and charges of $\mathbf{b_1}$ (cf. Table 3, entry 2, Supporting Information). A stabilizing two-electron, two-orbital interaction between the migrating C−H σ bond and the LUMO (p_{C1} in Figure 5)[2f,g] is possible in which the SOMO (p_{C3}) is not involved, as confirmed by the localization of spin density at the C_3 position in $\mathbf{TSe_1}$ (cf. Table 4, entry 2, Supporting Information). The stabilizing interaction is favored by the axial position of the migrating hydrogen. In the twisted conformer $\mathbf{b_1}$, the dihedral angle between the migrating C−H σ bond and the LUMO was estimated to be 21°, an almost parallel arrangement.

To confirm the preference for the planar 1,2 shift path I, we have calculated the energies of the transition structures for the

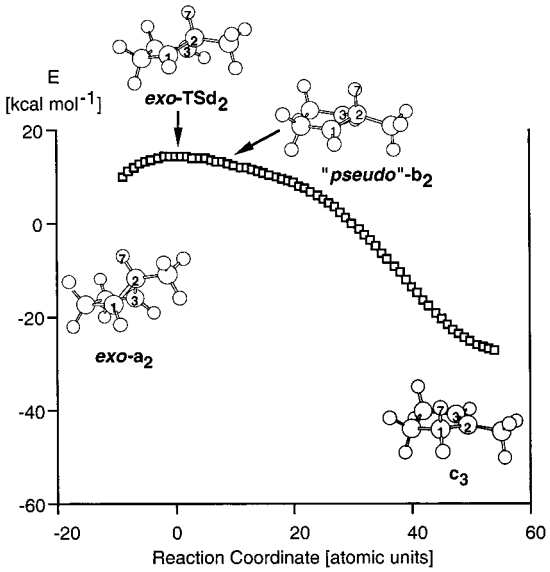

Figure 4. Intrinsic reaction coordinate (MP2/6-31G*) for the interconversion of ***exo*-a$_2$** and **c$_3$** through ***exo*-TSd$_2$**; the hydrogen migration starts when r_{1-3} has reached ca. 2.25 Å.

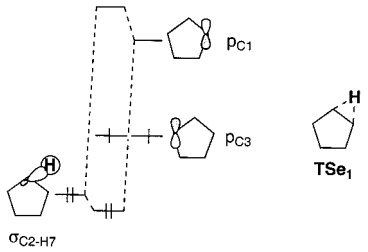

Figure 5. FMO interactions in the planar **TSe$_1$**.

alternative puckered migration (path IV in Scheme 2). For this path, we have studied the migration of the *endo* as well as of the *exo* substituent (R^1 and R^2 in Scheme 1). The activation energies for the corresponding ***endo*-** and ***exo*-TSf** (39−50 kcal mol^{-1}, cf. Table 4, Supporting Information) are considerably higher than the ones for the 1,2 rearrangement of the planar conformation (path I), whereas IRC calculations for the two puckered ***endo*-TSf$_1$** and ***exo*-TSf$_1$** confirmed that both TS's connect the puckered 1,3 radical cation **a$_1$** with the olefinic product **c$_1$**.

Let us now consider the unsymmetrical substrate **a$_3$** with methyl substitution at the bridgehead carbon (cf. Figure 6). The major effect of the methyl substituent in this position is the preferential stabilization of the positive charge, which forces spin localization on the unsubstituted carbon.[2c,g] Thus, the energy required for the breakage of the singly occupied bond via **TSd$_3$** is 3.0 kcal mol^{-1} (cf. Figure 6 and Table 4, entry 9, Supporting Information), which is substantially lower than the value of approximately 7 kcal mol^{-1} for the symmetric substrates **a$_1$** and **a$_2$**. Given the fact that the subsequent rearrangement, as we will discuss, is a low-barrier process, the lower bond-breaking energy explains the experimental finding that the 1,3 radical cation **a$_3$**, in contrast to **a$_1$** and **a$_2$**, does not persist, even in the 77 K matrix, to record its EPR spectrum.[2c]

In the planar intermediate **b$_3$**, the spin density is localized on the unsubstituted carbon atom. Our QCISD//MP2 calculations reproduce the experimental selectivity of the subsequent 1,2 rearrangement, with a barrier of 3.4 kcal mol^{-1} for the migration to the methyl-substituted cation site via **TSe$_3$** (cf. Table 4, entry 10, Supporting Information). This barrier is substantially lower than the one of 10.4 kcal mol^{-1} for the migration to the spin-bearing carbon via **TSe$_3$′** (cf. Table 4, entry 11, Supporting Information), which explains the formation of the thermodynamically less favored product **c$_2$** instead of **c$_3$**. Thus, our rationalization in terms of a Wagner−Meerwein rearrangement (migration of the hydrogen to a cationic carbon site, path I) is confirmed. A favorable two-electron, two-orbital interaction applies for the migration to the cationic center in the planar species, while the migration to the spin-bearing carbon atom requires an unfavorable three-electron, two-orbital interaction.

2.2. Loss of Selectivity through Dynamic Effects. Although our calculations have established the preference for the migration of the *endo* substituent, the 1,2 rearrangement of the *exo* substituent has been experimentally observed for the **a$_2$** derivative. Indeed, the 1,2 shift of the ***endo*-a$_2$** diastereomer was *endo* selective at 110 K, but some *exo* migration was detected at room temperature; i.e., the *exo*:*endo* ratio was 1:4 in favor of *endo* migration (cf. Scheme 1).[2b] This was previously explained in terms of conformational inversion of the ***endo*-a$_2$** to ***exo*-a$_2$** diastereomers, by which the bridge substituents R_1 and R_2 are interchanged, and a subsequent 1,2 shift of the originally *exo* substituent R_2 (cf. Scheme 2, path II). In view of our computational results, this explanation does not apply. Thus, state-averaged CASSCF calculations of the Jahn−Teller-like region of **CI$_2$** (cf. Supporting Information) have revealed that the invoked symmetric transition structure (the C_s-constrained minimum of the bonding $^2A'$ state) is a high-energy second-order saddle point (**SOSPa$_2$**, cf. Table 2, entry 15, Supporting Information).

Our present explanation is based on dynamic effects that may cause a "leak" in the reaction path I shown in Figure 4 for derivative ***exo*-a$_2$**. Thus, our IRC calculation shows that the reaction path passes through a planar structure, to which we refer as ***"pseudo"*-b$_2$**, in which the radical cationic carbon atoms are separated by approximately 2.25 Å and the 1,2 shift has not yet started. At planar geometries, two rearrangement paths (valleys on the potential energy surface) exist for **a$_2$**, where the migrating group is in an axial position: migration of the methyl group or of the hydrogen atom. Both reaction paths are separated by a low ridge, which may be surmounted by a rocking vibration of the methylene substituents that interchanges their axial and equatorial positions. This vibration corresponds to the imaginary frequency of **TSb$_2$** (the stationary point encountered along the derivative coupling coordinate **X$_2$** of **CI$_2$**, cf. Supporting Information). This imaginary frequency is analogous to the one of the unsubstituted **TSb$_1$** (cf. Figure 2c). Thus, **TSb$_2$** interconnects the two reaction paths for hydrogen and methyl shifts. The height of the energy barrier due to the ridge is estimated to be approximately 0.9 kcal/mol according to the value for the interconversion of **b$_1$** and **b$_1$′** via **TSb$_1$** at the MP2/6-31G* level of theory (cf. Table 3, entry 3, Supporting Information). This height is low enough to be surmounted at relatively high temperatures by virtue of the thermal energy of the molecule and gives rise to the observed "leak" in the stereoselectivity of the rearrangement. Moreover, the reaction path for methyl migration from the ***endo*-a$_2$** diastereomer should be higher in energy than the channel for hydrogen migration from ***exo*-a$_2$**, since the latter leads to the more stable product **c$_3$**. This explains that the selectivity loss at ambient temperature occurs only in the direction of ***endo*-** to ***exo*-a$_2$**. Detailed calculations of the dynamics for this process will be necessary to prove this hypothesis, but our presents results provide reasonable support.

Conclusions

In this work, we have shown how the Jahn−Teller-like degeneracy found for the cyclopentane-1,3-diyl radical cations

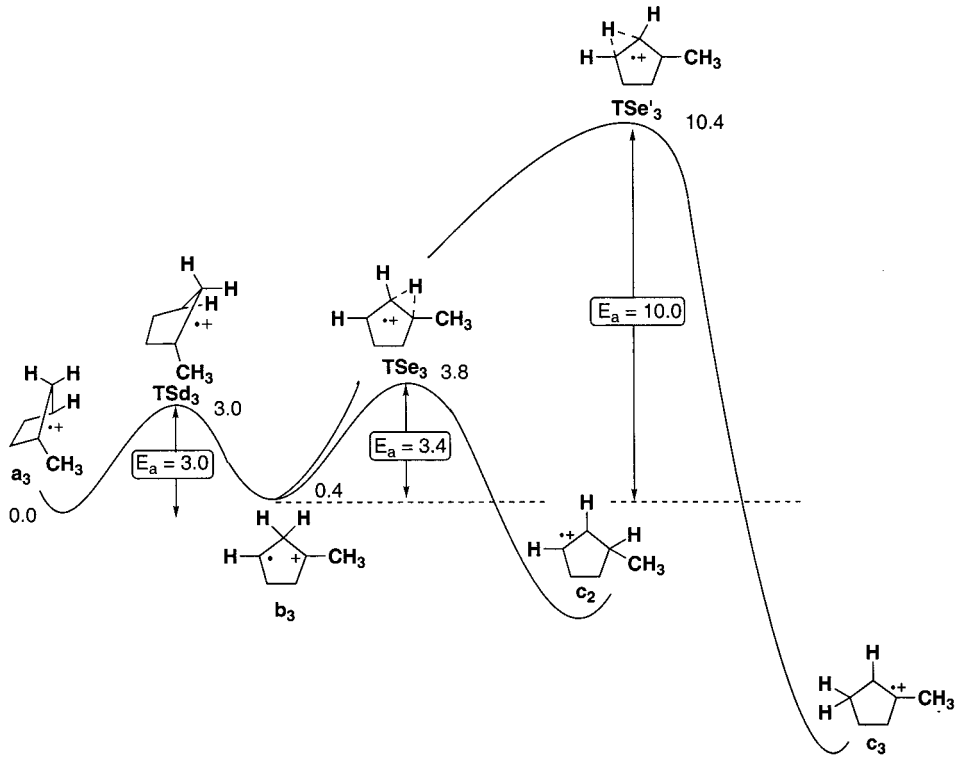

Figure 6. QCISD//MP2-631G* reaction coordinate for the 1,2 H shift of the bridgehead-substituted methyl substrate $\mathbf{a_3}$ (relative energies in kcal mol^{-1}).

$\mathbf{a_1}$ and $\mathbf{a_2}$ rationalizes the reactivity of these radical cations. Thus, the 1,2 rearrangement of the housane radical cations $\mathbf{a_1}-\mathbf{a_3}$ consists of two steps: opening of the puckered conformers along the bending coordinate $\mathbf{X_3}$, which leads to a planar intermediate **b** near the conical intersection, followed by the 1,2 shift from the planar intermediate **b** to the reaction products **c** along the coordinate $\mathbf{X_4}$. Mechanistically, the selectivity of the rearrangement can be explained with the help of intermediate **b**: on one hand, the migration proceeds to the carbon which bears the highest positive charge (Wagner−Meerwein rearrangement); on the other hand, it is the axial bridge substituent of **b** which migrates to account for the *endo* selectivity of the rearrangement. With our calculations of the Jahn−Teller moat that surrounds the conical intersection **CI**, we have established the preference for a localized intermediate rather than the symmetric transition structures for the conformational inversion and isomerization paths II and III. The derivative coupling coordinate provides the driving force for the electron localization and lowers the energy of the asymmetric structures **TSb** and **b**. In this respect, our potential energy surface topology resembles the "Bauld plateau" described for the ring-opening of bicyclobutane and cyclobutene radical cations.[3] We have proved here that the energy-lowering vibronic interactions are caused by the derivative coupling coordinate at the conical intersection, and we believe that this topology must have a more general validity for radical cations.

Computational Details

The CASSCF computations have been carried out with a development version of the Gaussian program.[16] The methods for state-averaged frequency[17] and CAS-MP2[18] computations have been implemented in this code. (For a more detailed discussion the reader is referred to the section Computational Details in the Supporting Information).

Acknowledgment. All computations were carried out on an IBM-SP2 funded jointly by IBM-UK and HEFCE (UK). We are grateful to Thomas Heidenfelder and Fumio Kita for helpful discussions. Financial support from the Volkswagen Stiftung, the Fonds der Chemischen Industrie, and the European Community for a Marie Curie Fellowship to L.B. (Grant No. ERB4001GT964926) is appreciated.

Supporting Information Available: Computational details, discussion of the Jahn−Teller surface for the bridge-substituted methyl derivative $\mathbf{a_2}$, Tables 2−5, and Cartesian coordinates and computed imaginary frequencies (MP2/6-31G* and CASSCF/6-31G* optimizations) of all structures reported (PDF). This material is available free of charge via the Internet at http://pubs.acs.org.

JA991441P

(16) All calculations were carried out with Gaussian 94, Revision B: Frisch, M. J.; Trucks, G. W.; Schlegel, H. B.; Gill, P. M. W.; Johnson, B. G.; Robb, M. A.; Cheeseman, J. R.; Keith, T.; Petersson, G. A.; Montgomery, J. A.; Raghavachari, K.; Al-Laham, M. A.; Zakrzewski, V. G.; Ortiz, J. V.; Foresman, J. B.; Cioslowski, J.; Stefanov, B. B.; Nanayakkara, A.; Challacombe, M.; Peng, C. Y.; Ayala, P. Y.; Chen, W.; Wong, M. W.; Andres, J. L.; Replogle, E. S.; Gomperts, R.; Martin, R. L.; Fox, D. J.; Binkley, J. S.; Defrees, D. J.; Baker, J.; Stewart, J. P.; Head-Gordon, M.; Gonzalez, C.; Pople, J. A. *Gaussian 94*, Revision B; Gaussian, Inc.: Pittsburgh, PA, 1995.

(17) Vreven, T. Ph.D. Thesis, University of London, 1998.

(18) González, D. Ph.D. Thesis, University of London, 1999.